Spectrochimica Acta Part A 77 (2010) 885–889

Contents lists available at ScienceDirect

Spectrochimica Acta Part A: Molecular and Biomolecular Spectroscopy

journal homepage: www.elsevier.com/locate/saa

Fabrication of Eu(III) complex doped nanofibrous membranes and their oxygen-sensing properties

Lin Songzhu[a,b], Dong Xiangting[a,*], Wang Jinxian[a], Liu Guixia[a], Yu Wenshen[a], Jia Ruokun[b]

[a] School of Chemistry and Environmental Engineering, Changchun University of Science and Technology, Changchun 130022, Jilin, PR China
[b] College of Chemical Engineering, Northeast Dianli University, Jilin 132012, PR China

ARTICLE INFO

Article history:
Received 6 May 2010
Received in revised form 11 July 2010
Accepted 4 August 2010

Keywords:
Optical materials
Composite materials
Europium compound
Chemical synthesis

ABSTRACT

In this paper, we report the synthesis, characterization, and photophysical properties of $Eu(TTA)_3ECIP$, where TTA = 2-thenoyltrifluoroacetonate, and ECIP = 1-ethyl-2-(N-ethyl-carbazole-yl-4-)imidazo[4,5-f]1,10-phenanthroline. Its elementary application for oxygen-sensing application is also investigated by doping it into a polymer matrix of polystyrene (PS). Experimental data suggest that the 2.5 wt% doped $Eu(TTA)_3ECIP$/PS nanofibrous membrane exhibits a high sensitivity of 3.4 towards oxygen with a good linear relationship of $R^2 = 0.9962$. In addition, the 2.5 wt% doped $Eu(TTA)_3ECIP$/PS nanofibrous membrane owns a quick response of 8 s towards oxygen, along with its excellent atmosphere insensitivity and photobleaching resistance. All these results suggest that both $Eu(TTA)_3ECIP$ and $Eu(TTA)_3ECIP$/PS system are promising candidates for oxygen-sensing optical sensors.

1. Introduction

The determination of molecular oxygen concentration in both gas and liquid phases is always an important analytical problem in many fields, such as chemical and food industries, medicine, analytical chemistry, and environmental monitoring [1,2]. Traditionally, oxygen concentration measurements are based on the Clark electrode and the Winkler titration approach which suffer from drawbacks such as oxygen consumption during sensing process, long response times and the tendency of electrodes to be poisoned by sample constituents [3,4]. In addition, both techniques necessitate sophisticated instrumentations and require complicated pretreatment procedures, making themselves unsuitable for on-line and/or in-field monitoring. Thus, the exploration for new oxygen-sensing systems has attracted considerable interests in the past decades.

Sensor technology is much simpler in instrumental implementation and sample preparation. Owing to the advantages of simple, rapid, and non-destructive characteristics, many oxygen-sensing systems have been reported. Among them, the development of optical oxygen sensors has attracted considerable attentions in recent years, as such sensors can offer advantages in terms of size, electrical safety, costs, not requiring a reference element, and the fact that analytical signals is free of influence from electromagnetic filed as well as easy to transmit over a long distance [5,6]. For practical applications, it is necessary to embed sensors into a solid matrix acting as a supporting medium, allowing oxygen transportation from surroundings. The commonly used matrixes are polymers, silica-based materials, and Langmuir–Blodgett films. Indeed, the support may have quite stringent criteria for suitable performances [7]. For example, a high diffusion coefficient is necessary for a rapid response, while, a highly locally effective quenching around the sensor molecule is necessary for good sensitivity, and long distance on-line monitoring necessitates a high degree of photostability. Thus, the exploration for sensors with intense luminescence, excellent antijam ability, high photostability, and good compatibility with supporting matrix is still a challenge for analytical chemistry.

It seems that rare-earth (RE)-based emitters which are usually excellent emitters can well satisfy the above requirements. Due to the unique excitation mechanism of antenna effect and *f–f* radiative transitions, RE^{3+}-based emitters can generate characteristically sharp and narrow emissions without being affected by surrounding environment or reagents, offering an excellent antijam ability. In addition, RE^{3+}-based emitters' good solubility in common solvents allow themselves to be easily embedded into supporting matrixes. All these excellent characters make RE^{3+}-based emitters promising candidates for oxygen-sensing materials. Guided by above results, in this paper, we report the synthesis, characterization, and photophysical properties of $Eu(TTA)_3ECIP$. Its elementary application for oxygen-sensing application is also investigated by doping it into a polymer matrix of PS. Experimental data suggest that both $Eu(TTA)_3ECIP$ and $Eu(TTA)_3ECIP$/PS system are promising candidates for oxygen-sensing optical sensors.

* Corresponding author. Tel.: +86 431 85583010.
E-mail address: xiangtingd@163.com (D. Xiangting).

1386-1425/$ – see front matter © 2010 Elsevier B.V. All rights reserved.
doi:10.1016/j.saa.2010.08.025

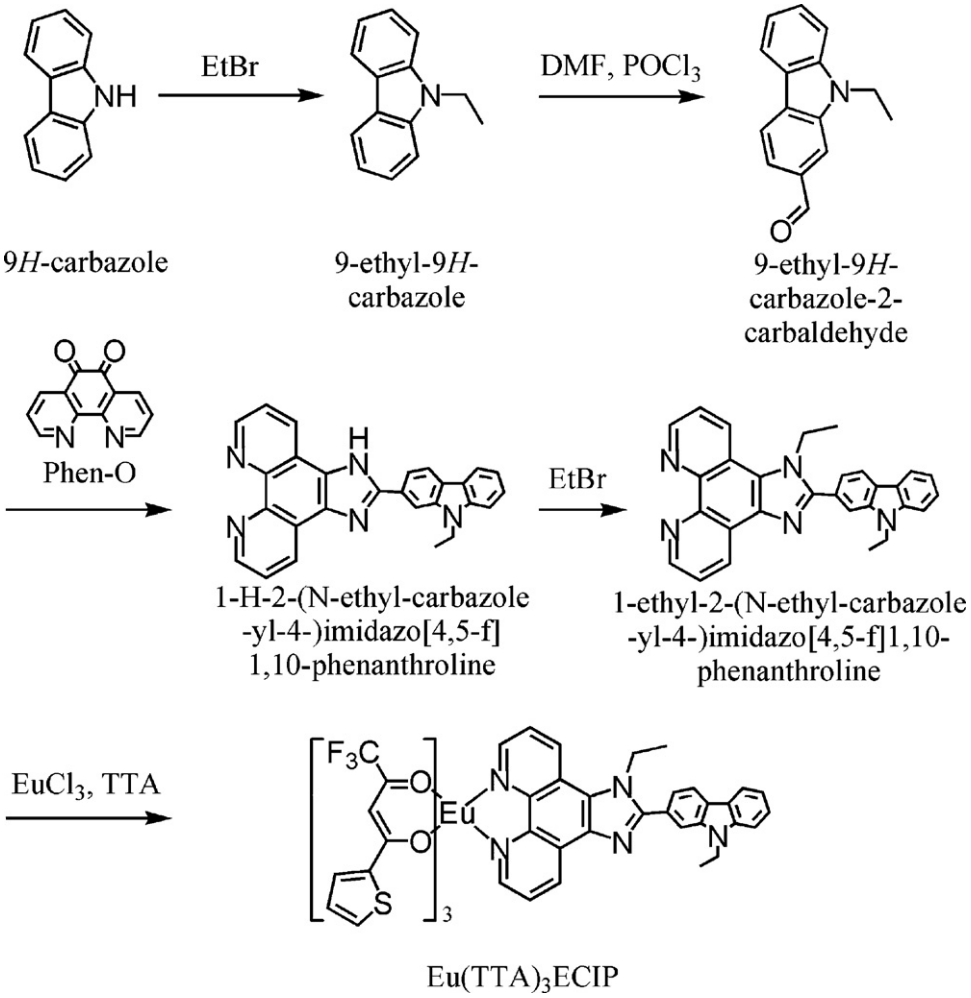

Scheme 1. A synthetic procedure for ECIP ligand and its corresponding Eu complex of $Eu(TTA)_3ECIP$.

2. Experimental

A synthetic procedure for the ligand of 1-ethyl-2-(N-ethyl-carbazole-yl-4-)imidazo[4,5-f]1,10-phenanthroline (referred as ECIP) and its corresponding Eu(III) complex with 2-thenoyltrifluoroacetonate (referred as TTA) as the auxiliary ligand is shown in Scheme 1.

1,10-Phenanthroline, TTA, 9*H*-carbazole, bromoethane, and polystyrene (referred as PS) were purchased from Aldrich Chemical Co. and used without further purifications. Organic solvents, including N,N′-dimethylformamide (DMF) and CH_2Cl_2, were purified through standard procedures. 1,10-phenanthroline-5,6-dione (referred as Phen-O) and 9-ethyl-9H-carbazole-2-carbaldehyde were synthesized according to literature procedures [7,8].

2.1. Synthesis of ECIP

The mixture of 10 mmol of 1,10-phenanthroline-5,6-dione, 10 mmol of 9-ethyl-9H-carbazole-2-carbaldehyde, 15.4 g of NH_4Ac, and 30 mL of HAc was stirred at 90 °C for 4 h. Then the mixture was poured into water and extracted with CH_2Cl_2. The crude product was used directly for next step without further purification. The mixture of 10 mmol of 1-H-2-(N-ethyl-carbazole-yl-4-)imidazo[4,5-f]1,10-phenanthroline, 10 mL of EtBr, and 0.3 g of NaH in 15 mL of DMF was stirred at 120 °C for 25 h. Then the mixture was poured into cold water and extracted with CH_2Cl_2, the crude product was purified by recrystallization from a mixture of CH_2Cl_2 and hexane to get yellow crystals. ^1H (300 MHz, $CDCl_3$), δ: 9.06 (2H); 8.94 (1H); 8.92 (1H); 8.63 (1H); 8.31 (1H); 7.88 (3H); 7.84 (1H); 7.82 (1H); 7.55 (1H); 7.28 (1H); 4.70 (2H); 4.55 (2H); 1.48 (3H); 1.41 (3H).

2.2. Synthesis of $Eu(TTA)_3ECIP$

$Eu(TTA)_3ECIP$ was synthesized according the literature procedure except that the auxiliary ligand was replaced by TTA [9]. Anal. Calcd. for $C_{53}H_{35}F_9O_6S_3N_5Eu$: C, 50.64, H, 2.81, N, 5.57. Found: C, 50.48, H, 2.89, N, 5.67.

2.3. Fabrication of $Eu(TTA)_3ECIP$/PS nanofibrous membranes

A typical procedure for the electrospinning composite nanofibers is described as follows. PS with a number-average molecular mass of 100,000 was dissolved in DMF to form a 22 wt% solution. Then $Eu(TTA)_3ECIP$ was added into the solution under stirring to form $Eu(TTA)_3ECIP$/PS homogeneous solutions. The final solutions were then electrospun to be composite nanofibrous membranes of $Eu(TTA)_3ECIP$/PS.

2.4. Measurements

Luminescence lifetimes were obtained with a 355 nm light generated from the Third-Harmonic-Generator pumped, using pulsed Nd:YAG laser as the excitation source. The Nd:YAG laser possesses

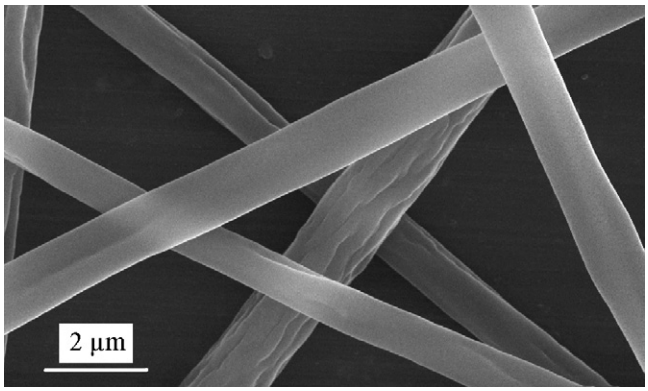

Fig. 1. A SEM image of the 2.5 wt% doped Eu(TTA)$_3$ECIP/PS nanofibrous membrane.

a line width of 1.0 cm^{-1}, pulse duration of 10 ns and repetition frequency of 10 Hz. A Rhodamine 6G dye pumped by the same Nd:YAG laser was used as the frequency-selective excitation source. All photoluminescence (PL) spectra were measured with a Hitachi F-4500 fluorescence spectrophotometer. UV–vis absorption spectra were recorded using a Shimadzu UV-3101PC spectrophotometer. Scanning electron microscopy (SEM) images were obtained on a Hitachi S-4800 microscope. ^{1}H NMR spectra were obtained with a Varian INOVA 300 spectrometer. Elemental analysis was performed on a Carlo Erba 1106 elemental analyzer. Oxygen-sensing performances were measured on the basis of steady emission intensity quenching. All measurements were carried out in the air at room temperature without being specified.

3. Results and discussion

3.1. Morphology of Eu(TTA)$_3$ECIP/PS nanofibrous membranes

For practical applications in optical oxygen-sensing devices, it is necessary to embed sensors into a solid matrix acting as a supporting medium, allowing oxygen transportation from surroundings, and the supporting medium may also have quite stringent criteria for suitable performances. Here, we select PS which has been proved to be an excellent host material for electrospinning as the supporting matrix for our primitive research [10]. To begin with, we try four dopant concentrations of 1.5, 2, 2.5, and 3 wt%, respectively. Fig. 1 shows a typical SEM image of the 2.5 wt% doped sample. The composite fibers with an average diameter of ~1 μm are randomly distributed on the substrate, showing a smooth and uniform morphology. No branch structure is observed for the composite fibers. Those composite fibers own a large surface-area-to-volume ratio which is two orders of magnitude larger than that of continuous thin films, providing an excellent matrix with high diffusion coefficient for a rapid response, which will be demonstrated later [10].

3.2. UV–vis absorption of Eu(TTA)$_3$ECIP/PS nanofibrous membranes

Fig. 2 shows the absorption spectra of the four samples with various dopant concentrations above mentioned. Compared with the absorption spectra of pure PS and pure Eu(TTA)$_3$ECIP shown in Fig. 2, it can be observed that each absorption spectrum of nanofibrous membranes is composed of two absorption bands: a high-energy band centering at ~260 nm originated from PS $\pi \rightarrow \pi^*$ transitions mixed with Eu(TTA)$_3$ECIP absorption, and a low-energy band peaking at ~350 nm which is attributed to TTA $\pi \rightarrow \pi^*$ transitions of Eu(TTA)$_3$ECIP complex. The absorption intensity at 350 nm increases with the increasing dopant concentrations. The absorption band shape, however, shows no spectral shift,

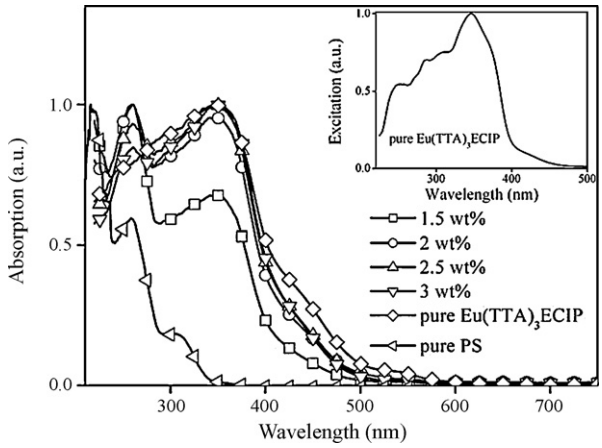

Fig. 2. Absorption spectra of pure PS, pure Eu(TTA)$_3$ECIP, and Eu(TTA)$_3$ECIP/PS nanofibrous membranes. Inset: a clear view for pure Eu(TTA)$_3$ECIP.

indicating that the increasing dopant concentrations and consequently the increasing intermolecular actions exert no obvious effect on molecular absorption. Correspondingly, the typical excitation spectrum of Eu(TTA)$_3$ECIP/PS nanofibrous membranes peaks at 348 nm, attributing to TTA $\pi \rightarrow \pi^*$ transitions. In addition, it is observed that there is a shoulder peak of 260 nm corresponding to PS $\pi \rightarrow \pi^*$ transitions, which means that there may be intermolecular energy transfer from PS matrix to Eu(TTA)$_3$ECIP molecules. Thus, we come to a conclusion that Eu(TTA)$_3$ECIP molecules are successfully embedded into PS matrix.

3.3. Photophysical properties of Eu(TTA)$_3$ECIP/PS nanofibrous membranes

Fig. 3 shows the PL spectra of the four samples upon excitation wavelength of 350 nm. Not surprisingly, character lines of Eu^{3+}, peaking at 577 nm for $^5D_0 \rightarrow {}^7F_0$, 590 nm for $^5D_0 \rightarrow {}^7F_1$, and 610 nm for $^5D_0 \rightarrow {}^7F_2$, respectively, are obtained. No emission the PS matrix is detected within the region from 400 to 750 nm, indicating that there is an efficiency energy transfer from PS to Eu(TTA)$_3$ECIP. According to the Judd–Ofelt theory, the radiative transitions within the [Xe]$4f^6$ configuration of Eu^{3+} are parity forbidden and consist mainly of weak magnetic dipole (MD) and induced electric dipole (ED) transitions [11]. The MD transition of $^5D_0 \rightarrow {}^7F_1$ is independent of the influence from micro-environment around Eu^{3+}. On the other

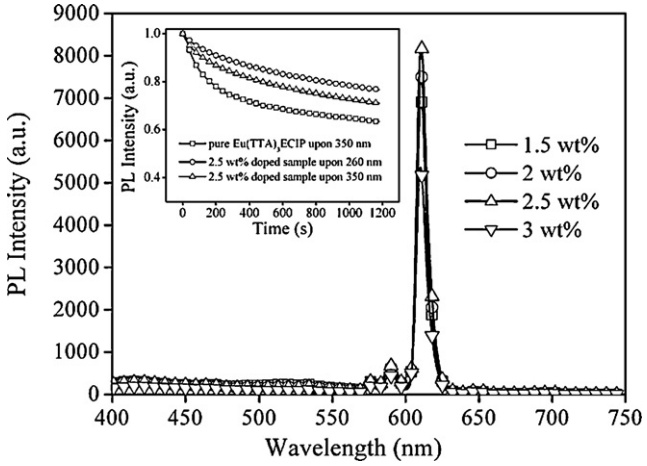

Fig. 3. PL spectra of the four samples upon excitation wavelength of 350 nm. Inset: emission intensity decay curves of the 2.5 wt% doped sample and pure Eu(TTA)$_3$ECIP powder upon excitation wavelength of 350 nm.

hand, the ED transition of $^5D_0 \rightarrow {}^7F_2$ is hypersensitive towards the micro-environment around Eu^{3+}. Since no spectral splitting is detected for both insensitive and hypersensitive transitions, it is thus estimated that all $Eu(TTA)_3ECIP$ molecules localize in a homogeneous micro-environment within PS matrix, which is critical for a good linear response and will be further confirmed later. In addition, it is observed that the micro-environment within PS matrix has no obvious influence on the emission peaks of $Eu(TTA)_3ECIP$ because the partially filled 4f orbitals are shielded from environment by the filled 5d and 5p orbitals, offering a good antijam ability towards environment effect.

As mentioned above, high photostability is a desired character for sensing materials. The inset of Fig. 3 demonstrates the emission intensity variations of the 2.5 wt% doped sample and pure $Eu(TTA)_3ECIP$ powder upon excitation wavelength of 350 nm. Clearly, both samples suffer from photobleaching caused by photo-induced structural decomposition. What's more, it is observed that the composite sample owns a largely improved photodurability compared with pure $Eu(TTA)_3ECIP$ powder, which can be explained as follows. The PS matrix may provide a rigid environment and thus a shield for $Eu(TTA)_3ECIP$ molecules, restraining the photo-induced structural decomposition. In addition, it is observed that the 2.5 wt% doped sample shows a better photodurability upon excitation wavelength of 260 nm compared with that under 350 nm radiation, which can be explained as follows. The PS absorption at 260 nm is stronger than that at 350 nm, consequently, the largely dominant matrix may transfer energy from PS matrix to $Eu(TTA)_3ECIP$ molecules upon excitation wavelength of 260 nm, which is also helpful for photodurability improvement of $Eu(TTA)_3ECIP$.

The $^5D_0 \rightarrow {}^7F_2$ emissions of the four samples follow an exhibit single-exponential decay pattern with lifetimes of 380 μs for the 1.5 wt% doped sample, 420 μs for the 2 wt% doped sample, 440 μs for the 2.5 wt% doped sample, and 420 μs for the 3 wt% doped sample, respectively. The $^5D_0 \rightarrow {}^7F_2$ luminescence lifetime shows an increase tendency with increasing concentrations from 1.5 to 2.5 wt%, which means that the intermolecular interaction between $Eu(TTA)_3ECIP$ molecules is so weak and the increasing concentrations of $Eu(TTA)_3ECIP$ molecules are positive to depress nonradiative decay within the matrix. Upon an even higher dopant concentration of 3 wt%, the $^5D_0 \rightarrow {}^7F_2$ luminescence lifetime tends to decrease due to the adverse intermolecular aggregation. Those long luminescence lifetimes make the samples vulnerable and sensitive towards energy-acceptors such as molecular oxygen. What is more, those long luminescence lifetimes make the elimination of fluorescence originated from surrounding impurity such as protein possible and practicable, offering an antijam ability towards fluorescence pollution.

3.4. Oxygen-sensing properties of $Eu(TTA)_3ECIP$/PS nanofibrous membranes

Considering the long luminescence lifetimes mentioned above, we intend to investigate their PL responses towards molecular oxygen and thus explorer the possibility of using $Eu(TTA)_3ECIP$/PS nanofibrous membranes as oxygen-sensing materials. According to the literature reports, molecular oxygen is an efficient killer for excited state emitters: energy transfer between molecular oxygen and excited state emitters happens, and the quenching mechanism is a dynamic one which can be presented as follows [7,12]:

$$Eu(TTA)_3ECIP* + O_2 \rightarrow Eu(TTA)_3ECIP + O_2* \quad (1)$$

where "*" indicates an excited state.

3.4.1. Sensitivity of $Eu(TTA)_3ECIP$/PS nanofibrous membranes

Fig. 4 shows the emission spectra of the 2.5 wt% doped sample under various oxygen concentrations from 0% to 100% with an interval of 10%. It is observed that the emission intensity at 610 nm decreases with the increasing oxygen concentrations. Here, oxygen sensitivity is defines as I_0/I_{100}, where I_0 is the luminescence intensity under 100% N_2 atmosphere and I_{100} is that under 100% O_2 atmosphere. The corresponding values for the four samples are measured to be 2.45 for the 1.5 wt% doped sample, 2.68 for the 2 wt% doped sample, 3.40 for the 2.5 wt% doped sample, and 2.57 for the 3 wt% doped sample. Correspondingly, the $^5D_0 \rightarrow {}^7F_2$ lifetimes for the four samples are measured to be 380 μs for the 1.5 wt% doped sample, 420 μs for the 2 wt% doped sample, 440 μs for the 2.5 wt% doped sample, and 420 μs for the 3 wt% doped sample. The 2.5 wt% doped sample exhibits a higher sensitivity and a longer lifetime than the others, which means that the sensitivity and the $^5D_0 \rightarrow {}^7F_2$ lifetime are not simply proportional to the loading concentration. It is thus reasonable to expect that there are at lest two opposite factors affecting sample sensitivity: emission intensity from probe molecules and adverse interaction between probe molecules (aggregation, for example). A low loading concentration leads to a weak emission from the probe and correspondingly the low sensitivity. On the contrary, a much higher loading concentration may result in the intermolecular aggregation which also decreases the sensitivity. This hypothesis is supported by the luminescence lifetimes analyses mentioned above. The two opposite factors may achieve a balance in the 2.5 wt% doped sample, resulting in the maximum sensitivity of 3.40.

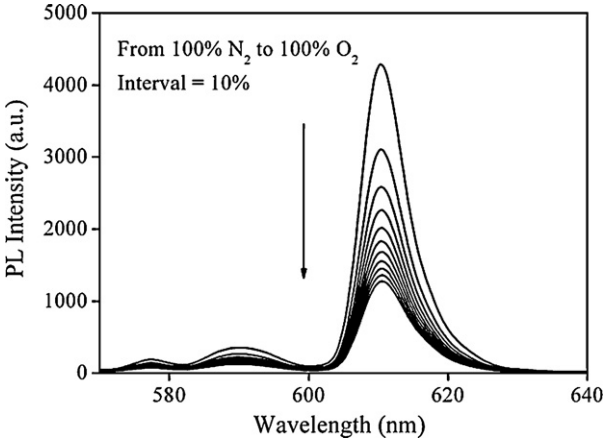

Fig. 4. Emission spectra of the 2.5 wt% doped sample under various oxygen concentrations from 0% to 100% with an interval of 10%.

Despite of the long $^5D_0 \rightarrow {}^7F_2$ lifetime of Eu^{3+} center (440 μs) as mentioned above, the samples' sensitivity values are much lower than those of sensing systems based on Ru^{2+} and Cu^+ complexes whose excited lifetimes are greatly shorter (<100 μs) [7,10]. It is expected that the luminescence mechanism difference between Eu^{3+}-based and Cu^+/Ru^{2+}-based emitters should be responsible for this phenomenon. As for typical Cu^+/Ru^{2+}-based emitters, the highest occupied molecular orbital has a predominant metal d character, while the lowest unoccupied molecular orbital is essentially π^* orbital of the ligands. Their emission corresponds to the lowest triplet T_1, and the excited state electron localizes on the ligands, which makes Cu^+/Ru^{2+}-based emitters open for molecular oxygen attack, leading to a high sensitivity. While, as for a Eu^{3+}-based emitter, the emission originates from metal-centered *f–f* transitions. The emissive center is covered by surrounding ligands and outer filled orbitals of Eu^{3+}, preventing molecular oxygen from closing in, leading to the low sensitivity, even though the excited state lifetime is much longer than those of Cu^+/Ru^{2+}-based emitters.

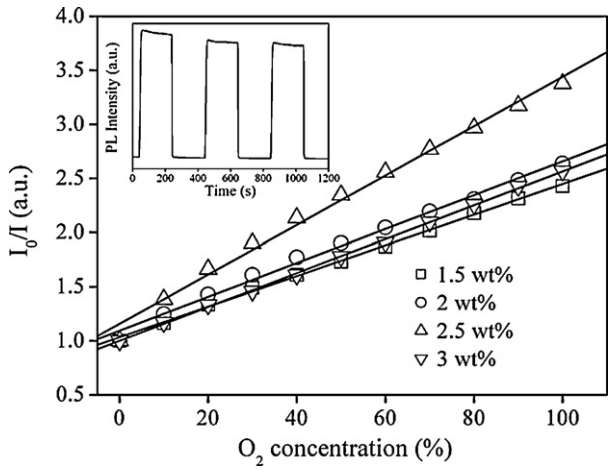

Fig. 5. Stern–Volmer plots of the four Eu(TTA)$_3$ECIP/PS nanofibrous membranes at various oxygen concentrations. Inset: PL intensity response of the 2.5 wt% doped sample when exposed to periodically varied 100% N_2 and 100% O_2 atmospheres.

Table 1
Oxygen-sensing properties of Eu(TTA)$_3$ECIP/PS nanofibrous membranes.

Sample (wt%)	I_0/I_{100} (a.u.)	K_{SV} ($O_2\%^{-1}$)	R^2	Response time (s)	Recovery time (s)
1.5	2.45	0.0142	0.9991	8	24
2	2.68	0.0156	0.9968	9	27
2.5	3.40	0.0228	0.9962	8	21
3	2.57	0.0156	0.9996	8	24

3.4.2. Stern–Volmer plots of Eu(TTA)$_3$ECIP/PS nanofibrous membranes

It has been reported that the quenching behavior of a probe is affected by the microstructure of matrix and the micro-environment in which the probe is located. Generally, in a homogeneous medium with a single-exponential decay, the intensity form of Stern–Volmer equation with dynamic quenching is described as follows [13]:

$$\frac{I_0}{I} = 1 + K_{SV}[O_2] \quad (2)$$

where I is luminescent intensity. The subscript 0 denotes a value in the absence of quencher, K_{SV} is the Stern–Volmer constant, and $[O_2]$ is O_2 concentration. A plot of I_0/I versus $[O_2]$ should be linear with identical slopes of K_{SV}. Fig. 5 shows the Stern–Volmer plots of the four samples at various oxygen concentrations. It is observed that all plots fit well with Eq. (1) and exhibit good linear relationships with increasing oxygen concentrations as depicted by Table 1. It is thus concluded that the micro-environment around Eu(TTA)$_3$ECIP molecules is homogenous and all Eu(TTA)$_3$ECIP molecules are uniformly distributed within PS matrix, which is consistent with the conclusion mentioned in Section 3.2.

3.4.3. Response/recovery time and photodurability of Eu(TTA)$_3$ECIP/PS nanofibrous membranes

Here, we define 95% response time as the time taken for a sample to lose 95% of its initial emission intensity when changed from 100% N_2 atmosphere to 100% O_2 atmosphere, and 95% recovery time as the time taken when changed from 100% O_2 atmosphere to 100% N_2 atmosphere. The corresponding values of the four samples are summarized in Table 1. The inset of Fig. 5 demonstrates a PL intensity response of the 2.5 wt% doped sample when exposed to periodically varied 100% N_2 and 100% O_2 atmospheres. Correspondingly, the 2.5 wt% doped sample renders a response time of only 8 s and a recovery time of 21 s. The quick response towards O_2 and N_2 suggests that the 2.5 wt% doped sample is highly sensitive towards O_2 due to the large surface-area-to-volume ratio of nanofibrous membranes as mentioned above. In addition, it is found that the recovery time is obviously longer than the response time, which can be explained by the diffusion-controlled dynamic response and recovery behavior of a hyperbolic-type sensor reported by Mills and Lepre [14]. The 2.5 wt% doped sample exhibits reversible time response plots, with slightly intensity decrease which is called photobleaching. For future studies, we are hoping to further improve the photostability and eliminate photobleaching by covalently grafting the probe into silica matrix.

4. Conclusion

In this paper, we report the synthesis, characterization, and photophysical properties of Eu(TTA)$_3$ECIP. Its elementary application for oxygen-sensing application is also investigated by doping it into a polymer matrix of PS. Experimental data suggest that the 2.5 wt% doped Eu(TTA)$_3$ECIP/PS nanofibrous membrane exhibits a high sensitivity of 3.4 towards oxygen with a good linear relationship of $R^2 = 0.9962$. In addition, the 2.5 wt% doped Eu(TTA)$_3$ECIP/PS nanofibrous membrane owns a quick response of 8 s towards oxygen, along with its excellent atmosphere insensitivity and photobleaching resistance. All these results suggest that both Eu(TTA)$_3$ECIP and Eu(TTA)$_3$ECIP/PS system are promising candidates for oxygen-sensing optical sensors.

Acknowledgement

Support of this research by the National Natural Science Foundation of China (Grant No. 50972020), the Research Project of Jilin Province (Grant No. 20070402, 20060504) and the Research Project of Changchun City (Grant No. 2007045).

References

[1] O.S. Wolfbeis, Anal. Chem. 80 (2008) 4269–4283.
[2] C. Baleizao, S. Nagl, M. Schaferling, M.N. Berberan-Santos, O.S. Wolfbeis, Anal. Chem. 80 (2008) 6449–6457.
[3] L.C. Clark Jr., Trans. Am. Soc. Artif. Intern. Organs 2 (1956) 41–48.
[4] L.W. Winkler, Ber. Dtsch. Chem. Ges. 21 (1888) 2843–2855.
[5] G. Zhang, J. Chen, S.J. Payne, S.E. Kooi, J.N. Demas, C.L. Fraser, J. Am. Chem. Soc. 129 (2007) 15728.
[6] A. Gulino, S. Giuffrida, P. Mineo, M. Purrazzo, E. Scamporrino, G. Ventimiglia, M.E. Van der Boom, I. Fragala, J. Phys. Chem. B 110 (2006) 16781–16786.
[7] B. Lei, B. Li, H. Zhang, L. Zhang, W. Li, J. Phys. Chem. C 111 (2007) 11291–11301.
[8] H. Xin, F.Y. Li, M. Guan, C.H. Huang, M. Sun, K.Z. Wang, Y.A. Zhang, L.P. Jin, J. Appl. Phys. 94 (2003) 4729–4731.
[9] L. Zhang, B. Li, J. Lumin. 129 (2009) 1304–1308.
[10] Y. Wang, B. Li, Y. Liu, L. Zhang, Q. Zuo, L. Shi, Z. Su, Chem. Commun. 39 (2009) 5868–5870.
[11] B.R. Judd, Phys. Rev. 127 (1962) 750–761.
[12] E.B. van der Tol, H.J. van Ramesdonk, J.W. Verhoeven, F.J. Steemers, E.G. Kerver, W. Verboom, D.N. Reinhoudt, Chem. Eur. J. 4 (1998) 2315–2323.
[13] X. Chen, Z.M. Zhong, Z. Li, Y.Q. Jiang, X.R. Wang, K.Y. Wong, Sens. Actuators B Chem. 87 (2002) 233–238.
[14] A. Mills, A. Lepre, Anal. Chem. 69 (1997) 4653–4659.